Pramana – J. Phys. (2024) 98:106
https://doi.org/10.1007/s12043-024-02760-z

Efficiency of the new B3Y-fetal potential in the analysis of the elastic and inelastic angular distributions for the ^{10}B+^{12}C system

N AMANGELDI[1,2], N BURTEBAYEV[1,2,3], S V ARTEMOV[4], MAULEN NASSURLLA[1,2,3], B MAUYEY[1,2], G YERGALIULY[1,2], MARZHAN NASSURLLA[1,2], F KH ERGASHEV[4], D SOLDATKHAN[1], D S SHAUDIRBAYEVA[1], AWAD A IBRAHEEM[5,6,*] and SH HAMADA[7]

[1]L.N. Gumilyov Eurasian National University, 010008 Astana, Kazakhstan
[2]Institute of Nuclear Physics, 050032 Almaty, Kazakhstan
[3]Al-Farabi Kazakh National University, 050040 Almaty, Kazakhstan
[4]Institute of Nuclear Physics, 100214 Tashkent, Uzbekistan
[5]Physics Department, King Khalid University, Abha, Saudi Arabia
[6]Physics Department, Al-Azhar University, Assiut Branch, Assiut 71524, Egypt
[7]Faculty of Science, Tanta University, Tanta, Egypt
*Corresponding author. E-mail: awad_ah_eb@hotmail.com

MS received 9 September 2023; revised 29 November 2023; accepted 6 February 2024

Abstract. In our previous work Burtebayev *et al, Int. J. Mod. Phys.* E **28**, 1950028 (2019), we presented the angular distribution (AD) for ^{10}B ions elastically scattered from the ^{12}C target at $E_{\rm lab}(^{10}\text{B}) = 41.3$ MeV. The measured data exhibited a pronounced increase in cross-sections at backward angles. This is mostly attributed to the effect of deuteron transfer between the colliding nuclei. In this work, we present the inelastic ADs for the same system leading to the $J^\pi = 2^+$, $E_x = 4.439$ MeV and $J^\pi = 3^-$, $E_x = 9.641$ MeV excited states of the ^{12}C nucleus. The measured inelastic ^{12}C(^{10}B, ^{10}B)^{12}C* ADs, together with the previously measured elastic ^{12}C(^{10}B,^{10}B)^{12}C ADs at $E_{\rm lab}(^{10}\text{B}) = 17.5$, 18, 41.3 and 100 MeV, are analysed within the methods of distorted wave Born approximation (DWBA) and coupled reaction channels (CRC) using the new B3Y and the standard M3Y effective interaction potentials. Spectroscopic amplitude (SA) values were determined for the $^{12}\text{C} \rightarrow {}^{10}\text{B} + d$ configuration.

Keywords. Elastic and inelastic scattering; B3Y-fetal folding potential; saturation property of nuclear matter; coupled channel method; distorted wave born approximation method; coupled reaction channel method.

PACS Nos **25.55.Ci; 24.10.Ht; 25.70.z; 25.45.Hi**

1. Introduction

Numerous theoretical frameworks have been devised to characterise the real and imaginary components of the nuclear interaction potential, aiming to effectively account for a diverse range of elastic scattering measurements at various energies [1–4]. Elastic scattering is a fundamental process in nuclear reactions that provides valuable insights into the properties of the interacting nuclei, including their binding nature, deformation parameters and spectroscopic factors. Furthermore, the investigation of elastic processes may present significant difficulties in cases where the coupling effects to nonelastic channels are substantial. Specifically, in nuclear processes induced by weakly bound (WB) projectiles, the dynamics of the reaction can be influenced by direct mechanisms such as breakup or transfer. This is mostly due to their low breakup threshold energy [5–9].

Traditionally, the optical model (OM), based on simplifying the solution of Schrödinger's equation that describes the scattering process by replacing the N-body problem (N is the total number of nucleons in the interacting nuclei) with a one-body problem of a reduced mass (μ) and moving in a potential well created by all nucleons, was employed successfully to reproduce a large body of scattering data. For resolving the parameter ambiguities that are normally associated with the traditional Woods–Saxon (WS) optical potentials, the double folding model (DFM) was extensively

Published online: 29 July 2024

employed. In a comprehensive investigation, Satchler and Love [10] employed the microscopic M3Y sum of three Yukawa nucleon–nucleon potentials, using matter radii obtained from electron scattering data when accessible, to examine the potential existence of a universal method for generating interaction potentials. According to the analysis of elastic scattering processes, it is feasible to increase the saturation of the nuclear medium in addition to acquiring essential information on the structure of the nucleus and the reaction mechanism. The saturation point of the dependence of the binding energy of the nucleus on density is directly related to nuclear incompressibility (K) [11]. In the study of the scattering process, the method of constructing the equation of state of the nucleus based on considering the overlap of the density of the interacting nuclei is performed using a microscopic approach. The preparation of the effective nucleon–nucleon (V_{NN}) interaction potential, which depends on the density of both the projectile and the target, makes it possible to calculate the saturation property of nuclear matter (NM) [12].

One of the main aims of the current work is to check the reliability and effectiveness of the nucleon–nucleon interaction potential (V_{NN}) based on the B3Y-Fetal potential [11], recently constructed based on the calculation of the elements of the nuclear matrix of two bodies in a variational approach with lower-order constraints (LOCV) [13] in reproducing the considered ^{10}B $+^{12}$C elastic and inelastic angular distributions (ADs). As a reference guide, the most standard M3Y potential was employed also in the analysis. For this purpose, different interaction models, namely, CDM3Y2, CDB3Y2, CDB3Y3 and CDB3Y4, were tested to reproduce the considered data. These interaction models were chosen as they give very close nuclear incompressibility (K) value and hence very close results within these potentials are expected. The analysis emphasised the fact that higher value of NM incompressibility for a specific interaction implies a less attractive nature, necessitating a higher renormalisation factor.

The nuclear incompressibility is a fundamental key in our understanding of nuclear structure, reactions and the behaviour of NM. Determined through a combination of theoretical calculations and empirical models, K is influenced by the choice of the potential, such as the CDM3Y2, CDB3Y2, CDB3Y3 and CDB3Y4 interactions, used in these calculations. Typically falling within the range of 200 to 300 MeV, K values exhibit some variation and uncertainty. Certain studies have even suggested values below 200 MeV. The precise value of K has significant implications for the curvature of the binding energy curve, the saturation property of nuclear matter and the short-range behaviour of nuclear potentials. By adjusting the density dependence of the folding potential through the variations in K, researchers can achieve improved agreement with experimental scattering data, enabling a more comprehensive exploration of the properties displayed by atomic nuclei [14].

This work adds to the ongoing joint research program devoted to the investigation of the scattering processes at the DC-60 cyclotron, Institute of Nuclear Physics, Kazakhstan [15–20] and at the U-200P cyclotron, Warsaw University, Poland [21,22], in which the scattering processes are investigated to consider the influences of nucleon(s) transfer mechanism.

The structure of the paper is as follows: The experimental set-up is explained in §2. Section 3 is dedicated to the presentation of the implemented potentials. Section 4 provides an overview of the theoretical calculations, presents the obtained results and engages in a comprehensive discussion of the findings. A concise overview is provided in §5.

2. Experiment set-up

The ^{10}B ions beam of laboratory energy $E_{\rm lab} = 41.3$ MeV, was accelerated in the U-200P cyclotron, Warsaw University. The ^{10}B beam was impinged on a ^{12}C target foil of thickness $\sim$0.141 μg/cm^2. Four $\Delta E - E$ telescopes were employed for registering the reaction products. Each telescope consists of a silicon detector (E) of thickness $\sim$300 μm and an ionisation chamber (ΔE) filled with isobutene gas (C_4H_{10}). The measured elastic AD for the ^{10}B $+^{12}$C system at $E_{\rm lab} = 41.3$ MeV as well as more information on the experimental set-up and data acquisition are presented in our previous work [22]. The energy spectrum of the scattered ^{10}B ions from the ^{12}C target with transition to the $J^\pi = 2^+$, $E_x = 4.439$ MeV and $J^\pi = 3^-$, $E_x = 9.641$ MeV excited states of ^{12}C nucleus is shown in figure 1. The experimental ^{10}B + ^{12}C inelastic AD at $E_{\rm lab} = 41.3$ MeV is shown in figure 2.

3. Implemented potentials

There are a limited number of studies devoted to studying the ^{10}B $+^{12}$C nuclear system at $E_{\rm lab} = 17.5$ [23], 18 [24], 41.3 [22] and 100 MeV [25]. The measurements at low energies up to 41.3 MeV demonstrated the existence of an observed rise in differential cross-sections (DCs) at the backward hemisphere ($\theta > 90°$), which is attributed to deuteron transfer mechanism between the colliding nuclei, namely, ^{10}B and ^{12}C. In the aforementioned studies, the data in the forward hemisphere ($\theta < 90°$) were analysed using the phenomenological WS potential and to describe the AD data in the entire

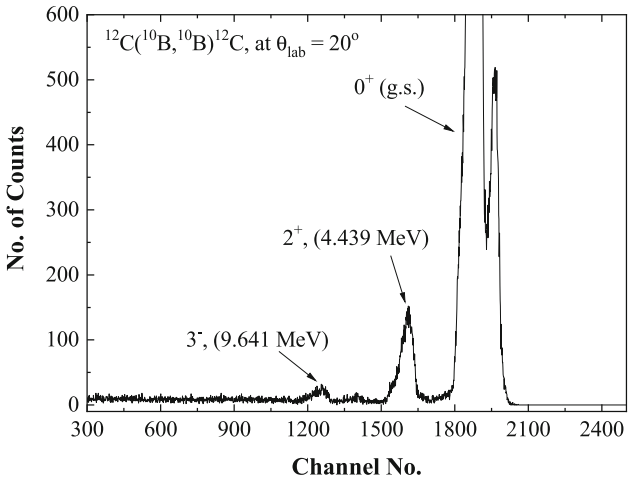

Figure 1. Energy spectrum of the ^{12}C(^{10}B, ^{10}B)^{12}C reaction products at $E_{\rm lab}(^{10}\mathrm{B}) = 41.3$ MeV and at angle $\theta_{\rm lab} = 20°$.

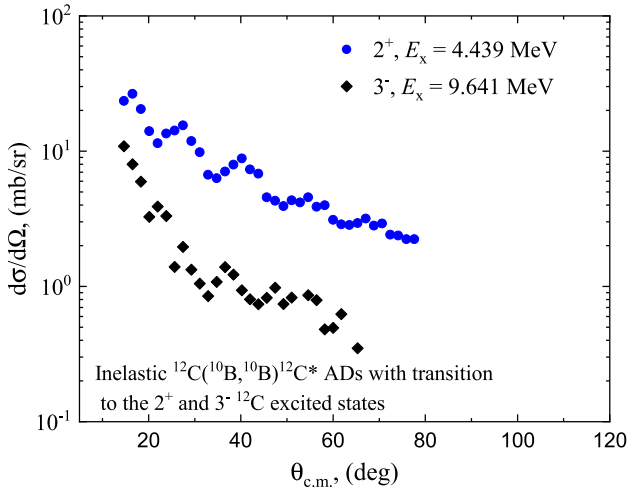

Figure 2. Experimental $^{10}\mathrm{B} + {}^{12}\mathrm{C}$ inelastic ADs at $E_{\rm lab}$ (^{10}B) = 41.3 MeV with transition to the $J^\pi = 2^+$, E_x = 4.439 MeV and $J^\pi = 3^-$, $E_x = 9.641$ MeV excited states of the ^{12}C nucleus.

angular range, the method of the distorted wave Born approximation (DWBA) was applied.

In this work, the elastic scattering ADs for the $^{10}\mathrm{B} + {}^{12}\mathrm{C}$ system at $E_{\rm lab}(^{10}\mathrm{B})$ between 17.5 and 100 MeV [22–25] are subjected to a microscopic analysis using a real double-folded (DF) potential based on both the new B3Y and the standard M3Y interaction potentials, each include both direct ($V^{\rm D}$) and exchange ($V^{\rm EX}$) components [14]. The real DF potential was estimated by folding the density distributions of the projectile ($\rho_{\rm P}(r_1)$) and of the target ($\rho_{\rm T}(r_2)$), with an effective potential [26,27] as follows:

$$V_{\rm DF}(R) = \iint \rho_{\rm P}(\vec{r}_1)\,\rho_{\rm T}(\vec{r}_2)\,V_{NN}(S)\,\mathrm{d}\vec{r}_1\mathrm{d}\vec{r}_2. \quad (1)$$

The direct and exchange components of the M3Y-Paris potential [28,29] are expressed as

$$v_{\rm D}(S) = \left[11061.625\frac{\exp(-4s)}{4s} - 2537.5\frac{\exp(-2.5s)}{2.5s}\right]\mathrm{MeV},$$

$$v_{\rm EX}(S) = \left[-1524.25\frac{\exp(-4s)}{4s} - 518.75\frac{\exp(-2.5s)}{2.5s} - 7.8474\frac{\exp(-0.7072s)}{0.7072s}\right]\mathrm{MeV}. \quad (2)$$

The direct and exchange components of the B3Y-Fetal [11] potential, based on the LOCV approach [13] are expressed as follows:

$$v_{\rm D}(S) = \left[10472.13\frac{\exp(-4s)}{4s} - 2203.11\frac{\exp(-2.5s)}{2.5s}\right]\mathrm{MeV},$$

$$v_{\rm EX}(S) = \left[499.63\frac{\exp(-4s)}{4s} - 1347.77\frac{\exp(-2.5s)}{2.5s} - 7.8474\frac{\exp(-0.7072s)}{0.7072s}\right]\mathrm{MeV}. \quad (3)$$

Direct and exchange potentials of the B3Y and M3Y types are formed depending on the density and energy [30].

$$v_{\rm D(EX)}(E,\rho,s) = F(E,\rho)g(E)v_{\rm D(EX)}(s), \quad (4)$$

the density-dependent function ($F(\rho)$) is expressed as [31],

$$F(\rho) = C\left[1 + \alpha\exp(-\beta\rho) - \gamma\rho^n\right] \quad (5)$$

and the energy-dependent factor ($g(E)$) is expressed as [32]

$$g(E) = 1 - 0.003(E/A). \quad (6)$$

Based on the adjustment of the density-dependent parameters in eq. (5), it is necessary to reduce the K-value in accordance with the saturation property of the nucleus. The parameters of the employed density-dependent function are listed in table 1.

By employing several parametrisations for the density dependency function, it is possible to obtain diverse models of interaction. Actually, it has been observed that various formulations of density dependence yield consistent NM saturation properties. However, they display distinct curvatures in the binding energy per nucleon (E/A) curve near the saturation point. This discrepancy

Table 1. Density-dependent parameters and incompressibility (K) values that are included in the B3Y-Fetal and M3Y-Paris potentials [11,14].

Density dependence	C	a	β (fm^3)	γ (fm^3)	K (MeV)
CDM3Y2-Paris	0.3346	3.0357	3.0685	1.0	204
CDB3Y2-Fetal	0.3346	3.0357	3.0685	1.0	204
CDB3Y3-Fetal	0.2985	3.4528	2.6388	1.5	217
CDB3Y4-Fetal	0.3052	3.2998	2.3180	2.0	228

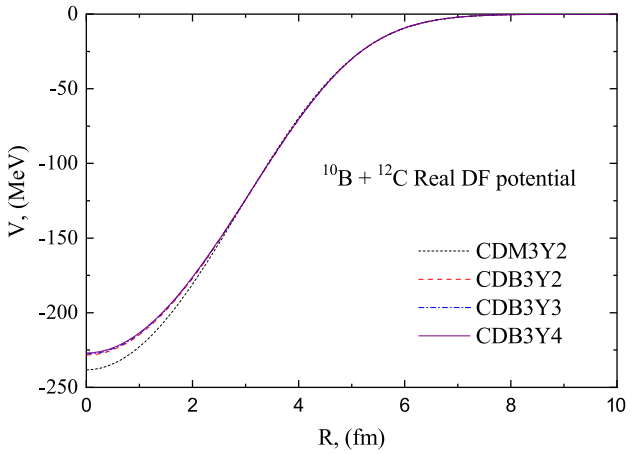

Figure 3. The generated real DF potentials for the ^{10}B+^{12}C system at $E_{\rm lab}(^{10}{\rm B}) = 41.3$ MeV using different interaction models.

is attributed to different values of the NM incompressibility (K), which is determined as

$$K = 9\rho^2 \frac{{\rm d}^2[E/A]}{{\rm d}\rho^2}\bigg|_{\rho=\rho_0}.$$

A higher value of NM incompressibility for a specific interaction implies a less attractive nature, necessitating a higher renormalisation factor. The distribution of matter density of the ^{10}B nucleus is expressed as

$$\rho(r) = \rho_0(1 + \alpha(r/a)^2)\exp(-(r/a)^2), \tag{7}$$

where $\rho_0 = 0.1593$, $a = 1.71$ and $\alpha = 0.837$ [33], while the density distribution of ^{12}C is expressed as

$$\rho(r) = \rho_0(1 + wr^2)\exp(-\beta r^2), \tag{8}$$

where $\rho_0 = 0.1644$, $w = 0.4988$ and $\beta = 0.3741$ [34].

The prepared real DF potentials for the ^{10}B + ^{12}C system at $E_{\rm lab}$ = 41.3 MeV utilising the so-called CDM3Y2, CDB3Y2, CDB3Y3 and CDB3Y4 interaction models are shown in figure 3. The generated DF potentials within CDB3Y2, CDB3Y3 and CDB3Y4 interactions are so close to each other, in the radial region >3 fm and the four generated potentials are nearly identical.

4. Results and discussion

4.1 *Elastic scattering* ^{12}C(^{10}B,^{10} B)^{12}C

The considered elastic scattering ADs for the ^{10}B + ^{12}C system at 17.5, 18, 41.3 and 100 MeV energies [22–25] are analysed using a real potential constructed according to the microscopic B3Y-Fetal and M3Y-Paris interaction potentials in addition to an imaginary part with the WS form, the so-called double-folding optical model (DFOM). The employed central potential has the following shape:

$$U(R) = V_{\rm C}(R) - N_{\rm R}V^{\rm DF}(R) - iW_0\left[1 + \exp\left(\frac{r - r_{\rm W}}{a_{\rm W}}\right)\right], \tag{9}$$

where $V_{\rm C}$ is the Coulomb potential of a uniformly charged sphere, $N_{\rm R}$ is the renormalisation factor of the real DF potential and the parameters W_0, $r_{\rm W}$ and $a_{\rm W}$ stand for the depth, radius parameter and diffuseness for the imaginary WS potential. The starting parameters of the imaginary WS potential part were chosen in accordance with previous studies [22–25] and were slightly adjusted to reduce the deviation between the experimental data and the theoretical calculations.

As a first step, we have performed the theoretical calculations in the forward angular region, $\theta < 90°$, to exclude the influence of the transfer, compound nucleus and other reaction channels on the potential parameters. In this case, the DCs are computed as the square of the elastic scattering amplitude $f_{\rm el}(\theta)$. The quality of fitting between the ^{10}B + ^{12}C elastic scattering ADs and the theoretical results using the DF potential, namely, CDM3Y2-Paris, CDB3Y2-Fetal, CDB3Y3-Fetal and CDB3Y4-Fetal interaction potentials, are fairly good, as depicted in figures 4 and 5 using the potential parametrisations presented in table 2.

In order to fit the experimental ADs in the entire angular range, the DWBA method was employed to consider the influence of deuteron transfer between the colliding nuclei, ^{10}B + ^{12}C. The main ingredient to perform the DWBA calculations is the optimal interaction potential, which fairly reproduces the experimental pure elastic scattering ADs in the forward angle

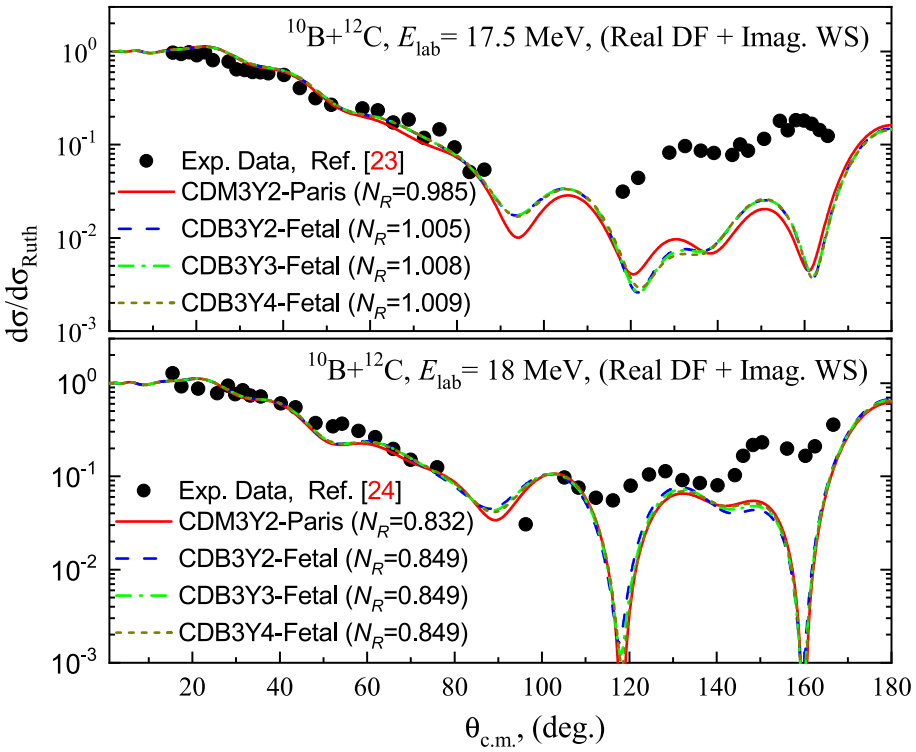

Figure 4. Experimental ADs (solid circles) vs. the theoretical results for the ^{12}C(^{10}B,^{10}B)^{12}C elastic scattering at $E_{lab} = 17.5$ and 18 MeV. The calculations are carried out using real DF potential of different interaction models, namely, CDM3Y2-Paris, CDB3Y2-Fetal, CDB3Y3-Fetal and CDB3Y4-Fetal in the forward hemisphere ($\theta_{c.m.} < 90°$). The imaginary potential has the conventional WS shape.

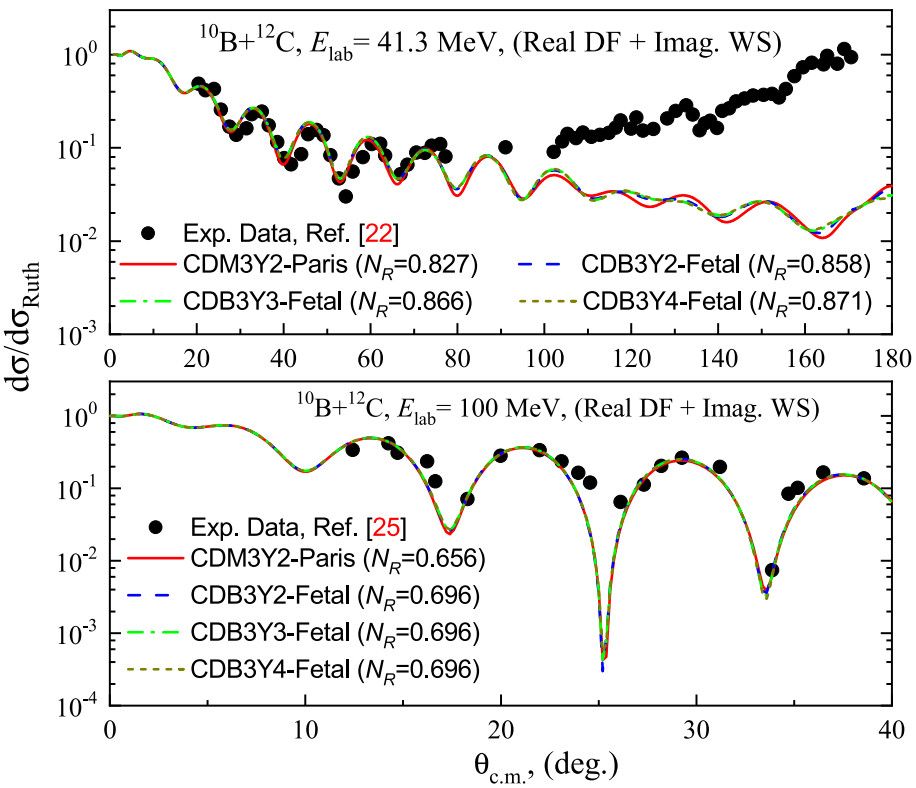

Figure 5. Same as figure 4 but at $E_{lab} = 41.3$ and 100 MeV.

Table 2. Parameters of the elastic and elastic transfer ADs for the $^{10}B + ^{12}C$ system at $E_{lab} = 17.5$, 18, 41.3 and 100 MeV within the framework of DFOM and DFM + DWBA, $r_C = 1.3$ fm.

E (MeV)	Interaction potential	Model	N_R	W_0 (MeV)	r_W (fm)	a_W (fm)	σ_R (mb)	SA	χ^2/N
17.5	CDM3Y2-Paris	DFOM	0.985	8.5	1.3	0.22	854.4		4.7
		DFOM+DWBA					848.9	1.8	4.2
	CDB3Y2-Fetal	DFOM	1.005	8.5	1.3	0.22	838.2		4.2
		DFOM+DWBA					831.8	1.8	4.2
	CDB3Y3-Fetal	DFOM	1.008	8.5	1.3	0.22	836.7		4.2
		DFOM+DWBA					830.3	1.8	4.2
	CDB3Y4-Fetal	DFOM	1.009	8.5	1.3	0.22	835.2		4.3
		DFOM+DWBA					828.7	1.8	4.3
18.0	CDM3Y2-Paris	DFOM	0.832	8.7	1.15	0.22	865.6		3.9
		DFOM+DWBA					856.3	1.6	18.8
	CDB3Y2-Fetal	DFOM	0.849	8.7	1.15	0.22	851.7		3.4
		DFOM+DWBA					841.7	1.6	22.8
	CDB3Y3-Fetal	DFOM	0.849	8.7	1.15	0.22	849.7		3.4
		DFOM+DWBA					839.9	1.6	21.9
	CDB3Y4-Fetal	DFOM	0.849	8.7	1.15	0.22	848.2		3.4
		DFOM+DWBA					838.5	1.6	21.3
41.3	CDM3Y2-Paris	DFOM	0.827	13.0	1.4	0.30	1229		9.1
		DFOM+DWBA					1226	1.64	18.5
	CDB3Y2-Fetal	DFOM	0.858	13.0	1.4	0.30	1224		10.8
		DFOM+DWBA					1222	1.64	20.6
	CDB3Y3-Fetal	DFOM	0.866	13.0	1.4	0.30	1225		10.9
		DFOM+DWBA					1222	1.64	18.6
	CDB3Y4-Fetal	DFOM	0.871	13.0	1.4	0.30	1224		11.0
		DFOM+DWBA					1222	1.64	18.6
100	CDM3Y2-Paris	DFOM	0.656	20.0	1.26	0.44	1311		12.8
	CDB3Y2-Fetal	DFOM	0.696	20.0	1.26	0.44	1312		12.2
	CDB3Y3-Fetal	DFOM	0.696	20.0	1.26	0.44	1311		12.2
	CDB3Y4-Fetal	DFOM	0.696	20.0	1.26	0.44	1311		12.3

Table 3. Cluster quantum numbers for the $^{12}C \rightarrow {}^{10}B + d$ configuration.

Overlap	N Number of nodes	L	S	$J = L + S$	B.E. (MeV)
$\langle {}^{12}C\,|{}^{10}B + d\rangle$	1	2	1	3	25.19

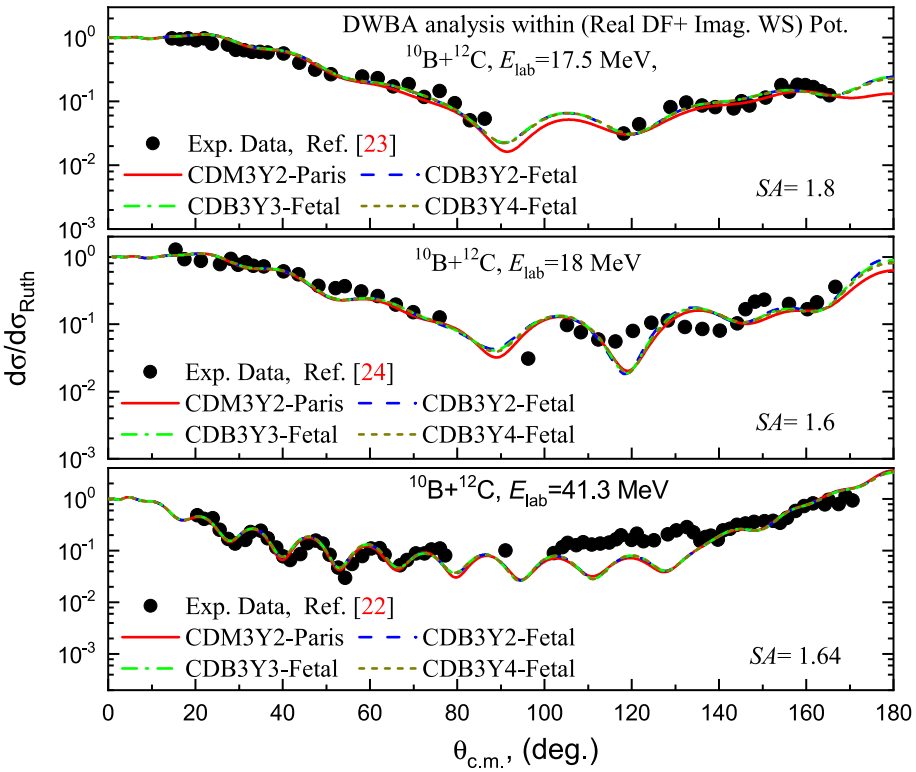

Figure 6. Experimental ADs (solid circles) vs. the theoretical results for the $^{12}C(^{10}B,^{10}B)^{12}C$ elastic transfer at $E_{lab} = 17.5$ [23], 18 [24] and 41.3 MeV [22]. The calculations within the DF + DWBA method were performed in the full angular range.

region (up to $\sim 90°$). Both the entrance ($^{10}B + {}^{12}C$) and exit ($^{12}C + {}^{10}B$) channels were considered to have the same potential due to their physical indistinguishability. The $d + {}^{10}B$ binding potential was taken in the usual WS shape of radius $r_V = 1.25$ fm, diffuseness $a_V = 0.65$ fm and the real potential depth was modified in order to accurately replicate the binding energy of the cluster ($E_b = 25.19$ MeV). All these potentials were fixed in the DWBA calculations and the only adjusting parameter is the SA, which was adjusted till the optimal consistency between the data and the results was reached by minimising the χ^2/N value. FRESCO and SFRESCO codes [35] were utilised to describe the data and get the optimal potential parameters.

As mentioned before, the DWBA calculations were performed to test the contribution of d transfer among the colliding nuclei. Such a transfer phenomenon results in an observed rise in DCs at backward angles. In this case, the DC can be expressed as the square sum of amplitudes for both elastic $f_{el}(\theta)$ and transfer $f_{DWBA}(\pi - \theta)$ as follows:

$$\frac{d\sigma_{el}}{d\Omega} = \left| f_{el}(\theta) + e^{i\alpha} S f_{DWBA}(\pi - \theta) \right|^2, \tag{10}$$

where S is the product of the two SA of the exchanged particle in the initial and final states which are identical in the case of elastic transfer. Cluster quantum numbers for the overlap $\langle {}^{12}C\,|{}^{10}B + d\rangle$ employed in the theoretical computations are presented in table 3. The number of nodes (N) was estimated utsing the Talmi–Moshinsky formula [36]:

$$2(N-1) + L = \sum_{i=1}^{n} 2(n_i - 1) + l_i, \tag{11}$$

where n_i, l_i are the quantum numbers of the transferred nucleons and L is the orbital moment of the cluster. The comparisons between the experimental ADs for

Table 4. Optimal parameters of the $^{10}B + ^{12}C$ system at $E_{lab} = 17.5$, 18, 41.3 and 100 MeV extracted from the CRC analysis using the (Real DF + Imag. DF) approach.

E (MeV)	Interaction potential	Model	NR	NI	σ_R (mb)	SA	χ^2/N
17.5	CDM3Y2-Paris	DF	1.02	0.074	880.4		3.3
		DF+CRC			883.8	1.67	6.31
	CDB3Y2-Fetal	DF	1.035	0.073	862.8		4.2
		DF+CRC			866.3	1.67	7.74
	CDB3Y3-Fetal	DF	1.038	0.073	861.4		4.3
		DF+CRC			858.8	1.67	8.62
	CDB3Y4-Fetal	DF	1.04	0.074	860.7		4.3
		DF+CRC			858.2	1.67	8.49
18.0	CDM3Y2-Paris	DF	0.744	0.319	875.9		1.3
		DF+CRC			870.2	2.13	11.9
	CDB3Y2-Fetal	DF	0.861	0.281	867.5		1.3
		DF+CRC			872.5	2.13	11.4
	CDB3Y3-Fetal	DF	0.869	0.281	867.3		1.3
		DF+CRC			872.3	2.13	11.4
	CDB3Y4-Fetal	DF	0.875	0.281	867.1		1.3
		DF+CRC			872.1	2.13	11.4
41.3	CDM3Y2-Paris	DF	0.732	0.102	1181		14.5
		DF+CRC			1180	1.26	14.4
	CDB3Y2-Fetal	DF	0.743	0.097	1168		14.1
		DF+CRC			1167	1.26	12.5
	CDB3Y3-Fetal	DF	0.745	0.097	1167		13.9
		DF+CRC			1166	1.26	13.7
	CDB3Y4-Fetal	DF	0.746	0.097	1166		13.9
		DF+CRC			1164	1.26	13.7
100	CDM3Y2-Paris	DF	0.577	0.482	1351		21.7
	CDB3Y2-Fetal	DF	0.615	0.505	1343		19.2
	CDB3Y3-Fetal	DF	0.619	0.508	1342		19.1
	CDB3Y4-Fetal	DF	0.622	0.511	1342		19.0

the $^{10}B + ^{12}C$ at $E_{lab} = 17.5$, 18 and 41.3 MeV and the theoretical results within the DWBA method using CDB3Y2-Fetal potential are depicted in figure 6. The SA for the $^{12}C \rightarrow {}^{10}B + d$ configuration was taken as a free parameter, which is adjusted to achieve the optimal consistency between the experimental data and the theoretical results as depicted in figure 7, which represents the variation of the extracted SA with χ^2/N at $E_{lab} = 17.5$, 18 and 41.3 MeV. The average extracted SA for the $^{12}C \rightarrow {}^{10}B + d$ configuration is 1.68 ± 0.106, which agrees well with the previously reported theoretical value of 1.78 [37,38]. The extracted SA values at the considered energies are displayed table 2.

Furthermore, we have examined the effect of absorption and coupling to other channels on the elastic and elastic transfer ADs for the considered $^{10}B + {}^{12}C$ system. First of all, to reduce the ambiguities from the phenomenological WS potential adopted for the imaginary part, we have reproduced the considered $^{10}B + {}^{12}C$ ADs within a real DF potential part in addition to an imaginary part taken as a factor multiplied by the real DF potential part. The previously utilised interaction models, namely, CDM3Y2, CDB3Y2, CDB3Y3 and CDB3Y4, were also employed. The central potential has the following shape:

$$U(R) = V_C(R) - N_R V^{DF}(R) - i N_I V^{DF}(R). \quad (12)$$

The considered data were fitted using only two adjustable parameters, namely, N_R and N_I, which stand for the normalisation factor for the real and imaginary DF potential parts, respectively. For simplicity, we shall call (Real DF + Imag. DF) potential approach. The N_R and N_I values were allowed to freely change till the best agreement between the data and the results were obtained and their optimal values are listed in table 4. It was found that the employed imaginary potential part plays a significant role in replicating the considered data especially at backward angles as shown in figures 8 and 9 when compared to the calculations within the DFOM (see figures 4 and 5).

Then, to examine the effect of channel coupling on the considered ADs data, the data were re-analysed

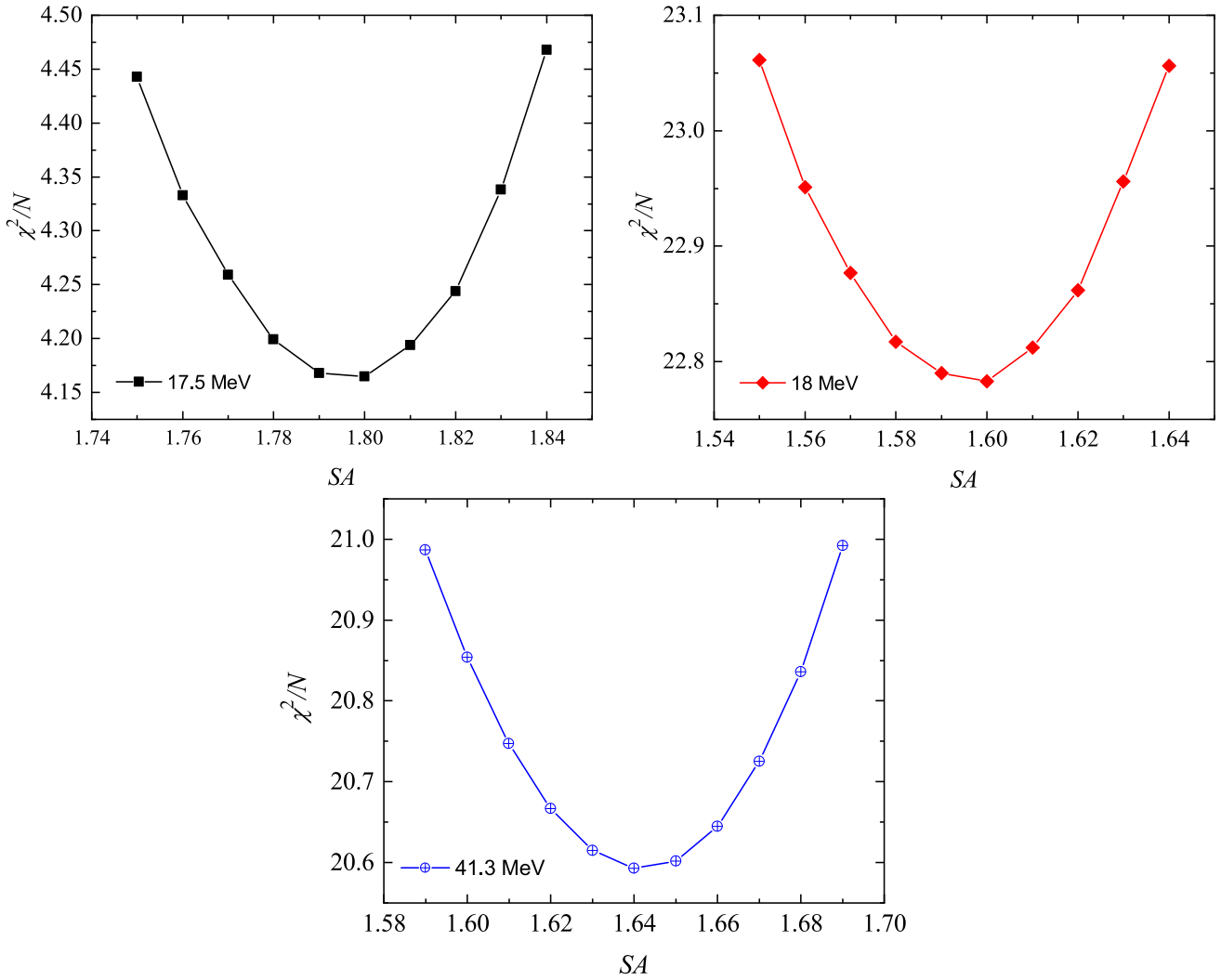

Figure 7. Variation of χ^2/N with the extracted SA from the theoretical calculations using DF (B3Y2-Fetal)+DWBA approach at $E_{\text{lab}} = 17.5$, 18 and 41.3 MeV.

within the framework of the CRC method. The CRC calculations were done using the optimal parameters obtained from the analysis within the Real DF + Imag. DF approach. The couplings to both the 2_1^+, $E_x = 4.439$ MeV and 3_1^-, $E_x = 9.641$ MeV ^{12}C excited state were considered with deformation parameters taken from ref. [39]. The comparison between the ^{10}B +^{12}C ADs data and the CRC calculations are shown in figure 10. The CRC calculations were performed using the same potentials for the ^{10}B + ^{12}C and ^{12}C + ^{10}B channels, listed in table 4, as they are physically indistinguishable. The optimal SA values for the ^{12}C $\rightarrow$ ^{10}B + d configuration extracted from the analysis within the CRC method were obtained by studying the variation between the χ^2/N and SA as shown in figure 11. Rather quite different SA values were extracted from the calculations within the CRC method (see table 4) to those obtained within the DWBA method (see table 2) at the same considered energies, which emphasises the high dependence of the SA values on both the utilised model and the interaction potential. The average extracted SA for the ^{12}C $\rightarrow$ ^{10}B + d configuration within the CRC method using the Real DF + Imag. DF potential is 1.69 ± 0.44, which agrees well with the previously reported theoretical value of 1.78 [37,38].

4.2 *Inelastic scattering* ^{12}C(^{10}B, ^{10}B)^{12}C*

A further test of the energy dependence of the implemented DF potentials extracted from the elastic scattering data is their use in reproducing the inelastic ^{10}B+^{12}C ADs data at $E_{\text{lab}} = 41.3$ MeV with transition to the 2_1^+, $E_x = 4.439$ MeV and 3_1^-, $E_x = 9.641$ MeV ^{12}C excited states within the coupled channels (CC) method.

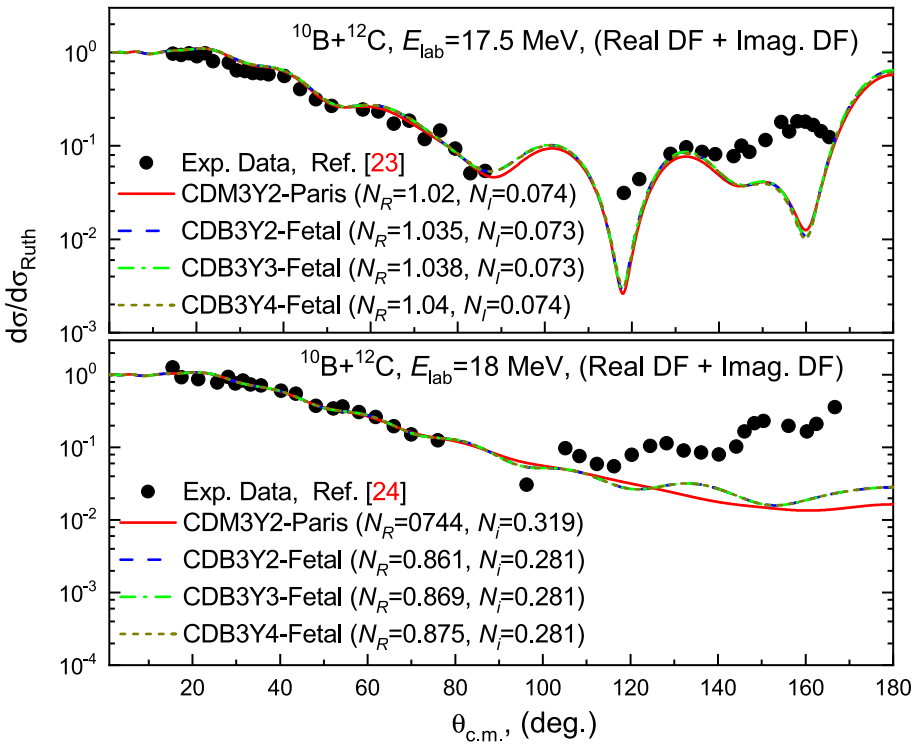

Figure 8. Experimental ADs (solid circles) vs. the theoretical results for the ^{12}C(^{10}B,^{10}B)^{12}C elastic scattering at $E_{lab} = 17.5$ and 18.0 MeV. The calculations are carried out using the (Real DF+Imag. DF) potential of different interaction models, namely, CDM3Y2-Paris, CDB3Y2-Fetal, CDB3Y3-Fetal and CDB3Y4-Fetal in the forward hemisphere ($\theta_{c.m.} < 90°$).

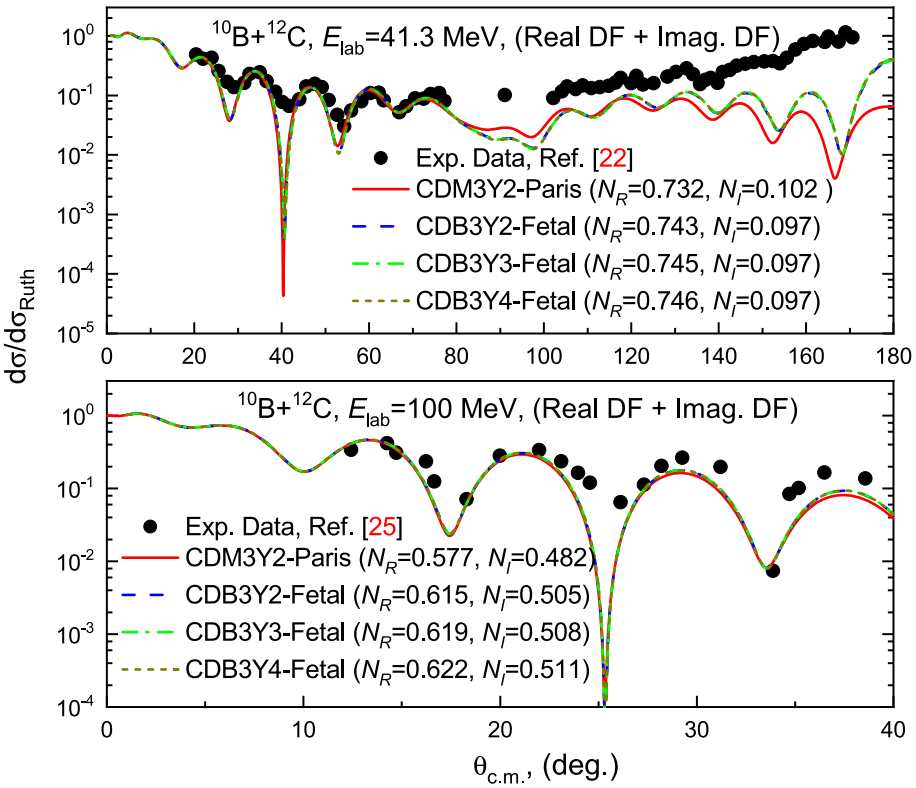

Figure 9. Same as figure 8 but at $E_{lab} = 41.3$ and 100 MeV.

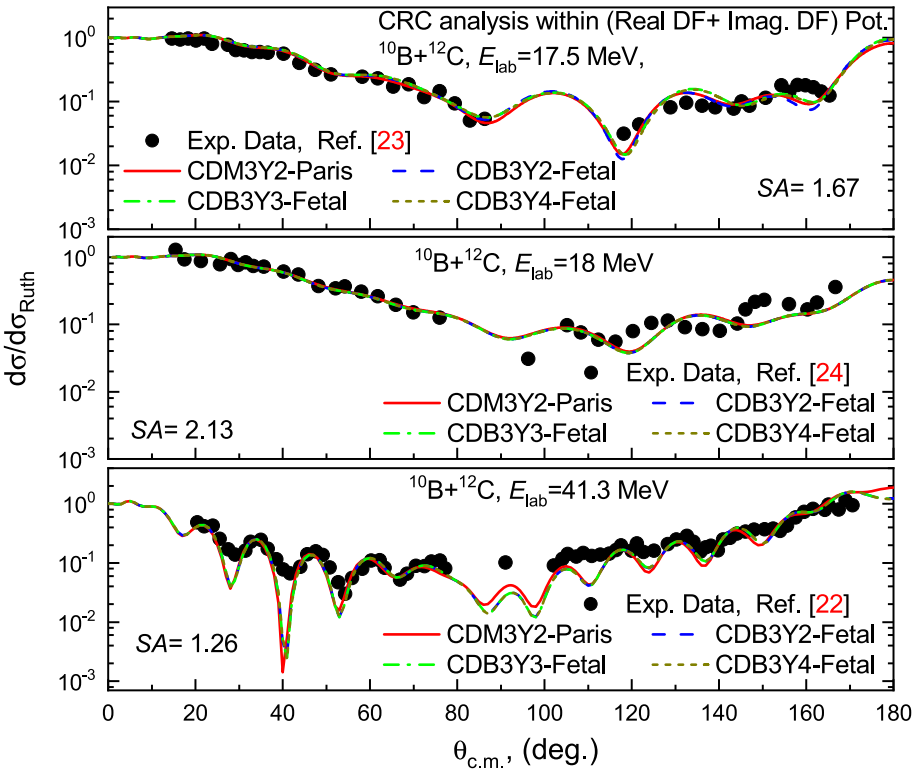

Figure 10. Experimental ADs (solid circles) vs. the CRC results for the ^{12}C(^{10}B,^{10}B)^{12}C elastic transfer at E_{lab} = 17.5, 18 and 41.3 MeV using the Real DF + Imag. DF potential approach.

The implemented quadrupole and octupole deformation parameters and lengths for the 2_1^+ and 3_1^- ^{12}C excited states in the CC calculations are displayed in table 5. As depicted in figure 12, the inelastic ^{12}C(^{10}B, ^{10}B)^{12}C* ADs agree reasonably well with the CC results. The nuclear potential was deformed utilising the deformation length (δ) given by $\delta_\lambda = \beta_\lambda \cdot R$, while the nuclear and Coulomb matrix elements in the rotational model are related by

$$M_n(E\lambda) = \frac{3Z\beta_\lambda R^\lambda}{4\pi}. \quad (13)$$

Here β is the deformation parameter and λ is the multipolarity. The transitions to these states were estimated using the form factor

$$V_\lambda(r) = -\frac{\delta_\lambda}{\sqrt{4\pi}}\frac{dU(r)}{dr} \quad (14)$$

5. Summary

We present the inelastic scattering ADs measurements for the ^{10}B + ^{12}C system leading to the $J^\pi = 2^+$, E_x = 4.439 MeV and $J^\pi = 3^-$, E_x = 9.641 MeV excited states of the ^{12}C nucleus. These measurements were performed at the U-200P cyclotron using ^{10}B ion beam with an energy of 41.3 MeV. These data were analysed within the CC method using real DF potential of different interaction models, namely, CDM3Y2-Paris, CDB3Y2-Fetal, CDB3Y3-Fetal and CDB3Y4-Fetal in addition to an imaginary WS potential. The aforementioned potentials were used to reproduce the previously measured elastic ^{12}C(^{10}B, ^{10}B)^{12}C and elastic transfer ^{12}C(^{10}B, ^{12}C)^{10}B ADs at 17.5, 18, 41.3 and 100 MeV energies. The marked increase in DCs at backward angles >90° for the three lowest studied energies emphasises that a significant contribution comes

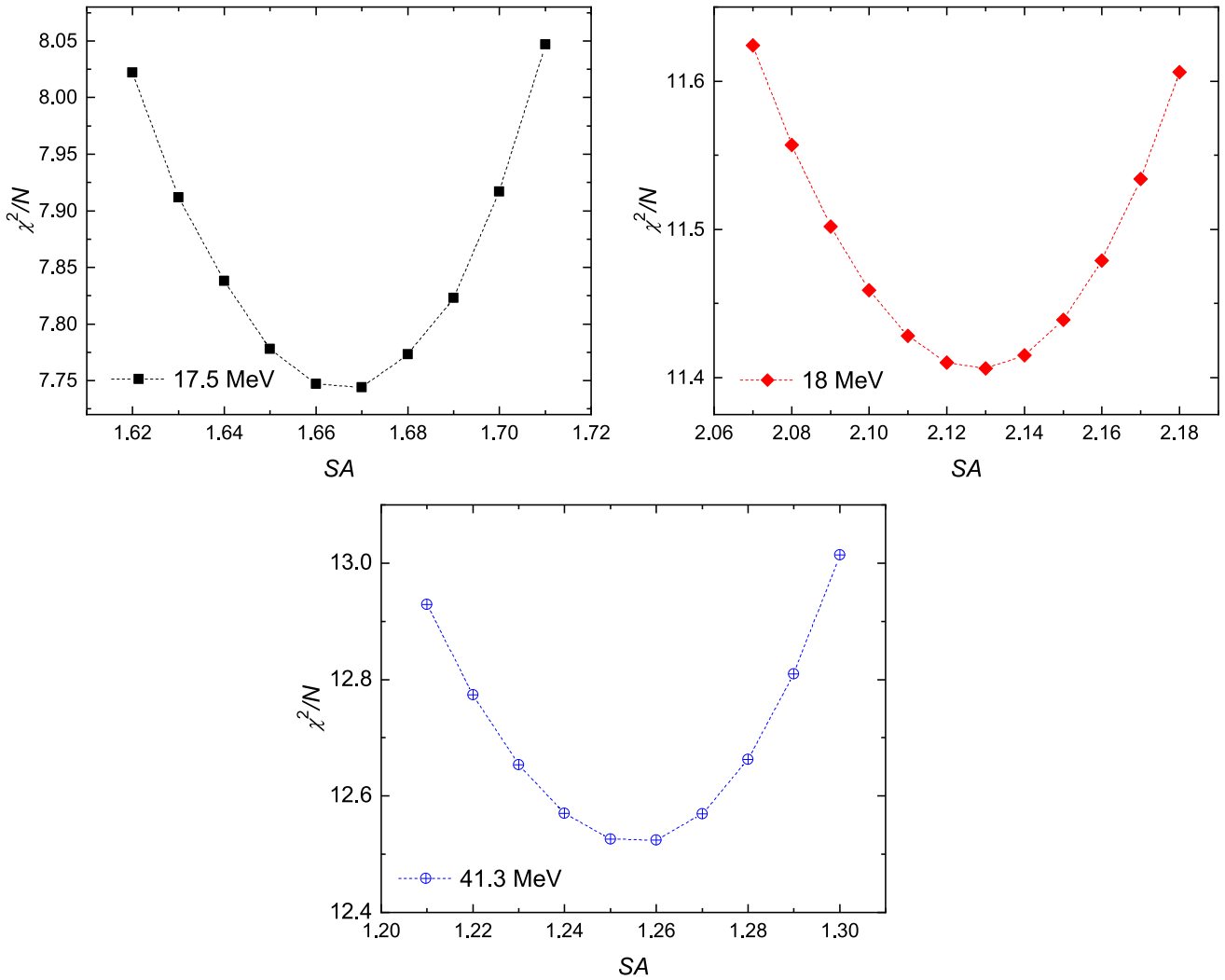

Figure 11. Variation of χ^2/N with the extracted SA from the CRC calculations at $E_{\text{lab}} = 17.5$, 18 and 41.3 MeV using the Real DF + Imag. DF potential approach based on the B3Y2-Fetal interaction model.

from deuteron transfer mechanism between the collided nuclei, ^{10}B and ^{12}C. The average extracted SA for the configuration $^{12}\text{C} \rightarrow {}^{10}\text{B} + d$ is 1.68 ± 0.106, which agrees well with the previously reported theoretical values [37, 38]. The extracted renormalisation factor, N_{R}, for the real DF potential using the aforementioned interaction models are close to each other. The effects may arise from the absorption and coupling to other channels on the $^{10}\text{B} + {}^{12}\text{C}$ elastic and elastic transfer ADs are further examined by employing another form for the imaginary potential rather than the previously employed WS form. In this case, the imaginary part was taken as a factor multiplied by the real part, the so called (Real DF+Imag. DF) potential approach. Within the CRC method, the considered data were re-analysed and the SA values were extracted, the average extracted SA within the CRC method is 1.69 ± 0.44. The analysis showed that the extracted SA values are strongly depending on both the employed potentials and calculation methods. The performed analysis gives evidence of the efficiency of the implemented B3Y-Fetal interaction potential in comparison with the standard M3Y potentials.

Table 5. The values of λ, β and δ for the 2^+ and 3^- ^{12}C excited states employed in the CC calculations.

State	Multipolarity (λ)	Deformation parameter (β)	Deformation length (δ)	Ref.
2^+_1	2	0.583	1.602	[39]
3^-_1	3	0.831	2.283	[39]

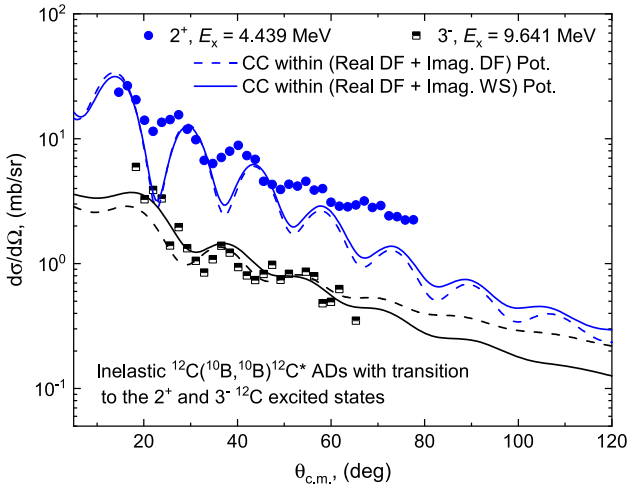

Figure 12. Inelastic ^{12}C(^{10}B, ^{10}B)^{12}C* scattering at $E_{\rm lab}$ = 41.3 MeV with transition to the $J^\pi = 2^+$, $E_x = 4.439$ MeV (circles) and $J^\pi = 3^-$, $E_x = 9.641$ MeV (squares) ^{12}C excited states. Solid curves denote the CC calculations using the Real DF+Imag. WS potential and dashed curves denote the CC calculations using the Real DF+Imag. DF potential.

Acknowledgements

The Science Committee of the Ministry of Science and Higher Education, Republic of Kazakhstan, has provided funding for this study (Grant No. AP14871692).

References

[1] G Satchler, *Phys. Rep*. **199**, 147 (1991)
[2] D T Khoa, *Nucl. Phys. A* **484**, 376 (1988)
[3] M Brandan and G Satchler, *Nucl. Phys. A* **487**, 477 (1988)
[4] M Brandan and G Satchler, *Phys. Rep*. **285**, 143 (1997)
[5] M A G Alvarez *et al*, *Phys. Rev. C* **98**, 024621 (2018)
[6] M Aversa *et al*, *Phys. Rev. C* **101**, 044601 (2020)
[7] Sh Hamada and A A Ibraheem, *Phys. Scr.* **97**, 125303 (2022)
[8] Sh Hamada and A A Ibraheem, *Nucl. Phys. A* **1030**, 122590 (2023)
[9] A Amar, K Rusek and Sh Hamada, *Eur. Phys. J. A* **59**, 182 (2023)
[10] G Satchler and W Love, *Phys. Rep*. **55**, 183 (1979)
[11] I Ochala and J O Fiase, *Phys. Rev. C* **98**, 064001 (2018)
[12] D T Khoa and W von Oertzen, *Phys. Lett. B* **342**, 6 (1995)
[13] J O Fiase, K R S Devan and A Hosaka, *Phys. Rev. C* **66**, 014004 (2002)
[14] D T Khoa *et al*, *Phys. Rev. C* **56**, 954 (1997)
[15] Sh Hamada *et al*, *Nucl. Phys. A* **859**, 29 (2011)
[16] Sh Hamada, N Burtebayev and N Amangeldi, *Int. J. Mod. Phys. E* **22**, 1350058 (2013)
[17] Sh Hamada, N Burtebayev and N Amangeldi, *Int. J. Mod. Phys. E* **23**, 1450061 (2014)
[18] N Burtebayev *et al*, *Acta Phys. Pol. B* **48**, 495 (2017)
[19] N Burtebayev *et al*, *Acta Phys. Pol. B* **50**, 1423 (2019)
[20] Marzhan Nassurlla *et al*, *Chin. Phys. C* **44**(**10**), 104103 (2020)
[21] M Nassurlla *et al*, *Eur. Phys. J. A* **57**, 231 (2021)
[22] N Burtebayev *et al*, *Int. J. Mod. Phys. E* **28**, 1950028 (2019)
[23] N Amangeldi *et al*, *Acta Phys. Pol. B* **51**, 757 (2020)
[24] U C Voos, W Von Oertzen and R Bock, *Nucl. Phys. A* **954**, 207 (1969)
[25] C W Towsley *et al*, *Phys. Rev. C* **15**, 281 (1977)
[26] G Bertsch, J Borysowicz, H McManus and W G Love, *Nucl. Phys. A* **284**, 399 (1977)
[27] B S Sinha, *Phys. Rep*. **20**, 1 (1975)
[28] D T Khoa *et al*, *Phys. Rev. Lett*. **74**, 34 (1995)
[29] D T Khoa and G R Satchler, *Nucl. Phys. A* **668**, 3 (2000)
[30] D T Khoa, W von Oertzen and H G Bohlen, *Phys. Rev. C* **49**, 1652 (1994)
[31] G Bertsch *et al*, *Nucl. Phys. A* **284**, 399 (1977)
[32] DT Khoa and W Von Oertzen, *Phys. Lett. B* **304**, 8 (1993)
[33] H De Vries, C W De Jager and C De Vries, *At. Data Nucl. Data Tables* **36**, 495 (1987)
[34] S Qing-biao, F Da-chun and Z Yi-Zhong, *Phys. Rev. C* **43** 2773 (1991)
[35] I J Thompson, *Comput. Phys. Rep*. **7**, 167 (1988)
[36] B Buck and A A Pilt, *Nucl. Phys. A* **280**, 133 (1977)
[37] A A Rudchik *et al*, *Eur. Phys. J. A* **23**, 445 (2005)
[38] V M Kyryanchuk *et al*, *Nucl. Phys. A* **726**, 231 (2003)
[39] P Möller, A J Sierk, T Ichikawa and H Sagawa, *At. Data Nucl. Data Tables* **109–110**, 1 (2016)